DISEASES AND DISORDERS

Apolipoprotein E drives microglia activation in the development of autoimmune uveitis through up-regulation of peptidyl prolyl isomerase F

Shuhao Zeng[1]†, Yakun Wang[1,2]†, Xianyang Liu[1], Hui Feng[1], Fan Cao[1], Baorui Chu[1], Chao Wu[1], Wei Fan[3], Ke Hu[3], Fengyang Lei[1]*, Shengping Hou[1]*

Autoimmune uveitis (AU) is a category of sight-threatening diseases with different pathological causes. Transcriptomic analysis of patients with AU revealed a highly oxidative stress profile as well as an up-regulated *apolipoprotein E* (*APOE*) expression in their peripheral blood mononuclear cells (PBMCs). In addition, single-cell RNA sequencing of retinal microglia also identified an up-regulated expression of *APOE* in a murine model of experimental AU (EAU). Our results and others previously suggested that microglia are tightly associated with the development of AU. Meanwhile, although *APOE* has been reported to play a myriad of functions ranging from lipid metabolism to neural regeneration, little is known about its detailed mechanism in the development of AU. In this study, a murine EAU model was used to investigate the association between *APOE*, microglia, and EAU, and it is found that *APOE* is indispensable for EAU induction as *APOE*$^{-/-}$ mice failed to develop EAU. In vitro studies using microglial cells further demonstrated that *APOE* is positively corelated with microglial inflammation, which could be reversed by knocking down *APOE* using short hairpin RNA. Proteomic analysis indicated that *APOE*-mediated microglial activation relies on reactive oxygen species (ROS) pathway, through *peptidyl prolyl isomerase F* (*PPIF*), which was further verified in PBMCs derived from patients with AU. Supplementation of *PPIF* reverses *APOE* deficiency–caused ROS activation in vitro. In addition, Adeno-associated virus-mediated overexpression of *PPIF* exacerbated EAU phenotype, suggesting its important role in driving uveitis initiation. These results provide an understanding of *APOE* and *PPIF* in the pathogenesis of uveitis.

INTRODUCTION

Autoimmune uveitis (AU) is a common ocular disease that affects multiple segments of the eye, primarily the uvea and choroid, and is caused by dysregulated ocular immune homeostasis. Clinically, it manifests with a combination of different signs such as conjunctival hyperemia, ciliary congestion, posterior synechiae, and, most prominently, pain (*1*). Patients with AU also frequently present with systemic symptoms, including psoriasis, arthritis, and vasculitis; thus, it is equivalently important to treat AU as well as other autoimmune diseases (*2*–*4*). However, current clinical management of AU primarily focuses on symptomatic relief using corticosteroids and immunosuppressants (*5*). Thus, decrypting the etiologic mechanisms would help develop a targeted therapy for AU.

Previous studies have shown the breakdown of the blood-retinal barrier (BRB) (*6*), dysfunction of peripheral T cells (*7*, *8*), and the activation of retinal microglia (*9*, *10*), all of which are associated with the disease progression of uveitis. Accumulating evidence suggests that microglia play a pivotal role in the pathogenesis of uveitis, with their aberrant activation exacerbating pan-ocular inflammation (*11*). Furthermore, classical experimental AU (EAU) failed to be induced in PLX5622-treated mice, a small-molecule CSF1R inhibitor that blocks CSF1R signaling and thus depletes microglia (*12*). Hence, understanding the detailed role of microglia in uveitis development would generate previously unknown information for defining novel targets in uveitis management.

Microglia are recognized as a group of highly specialized resident immune cells within the central nervous system (CNS), including the retina, where they perform multifaceted functions in maintaining physiological homeostasis and modulating local neuroinflammation (*13*). Under physiological conditions, retinal microglia, as the sole resident immune cells, survey the retinal microenvironment and maintain its wellness and integrity (*14*). Morphologically, quiescent state microglia have a ramified shape, which facilitates communication with neurons and other cells (*15*). Under pathological conditions, microglia often undergo a phenotypic switch from ramified to ameboid-like, accompanied by production and secretion of proinflammatory cytokines, such as tumor necrosis factor–α (TNF-α) and interleukin-6 (IL-6) (*16*). This transition leads to a further disruption of the BRB and the recruitment of peripheral immune cells, ultimately exacerbates the inflammatory response, and promotes the development of uveitis.

Apolipoprotein E (*APOE*) is a member of the vertebrate exchangeable apolipoprotein family, comprising 299 amino acids and featuring an amphiphilic helix encoded by multiple nucleotide tandem repeats, which plays a crucial role in lipoprotein metabolism and immune regulation (*17*). Recent studies have demonstrated a notable association between *APOE* and the formation of amyloid-β precursor protein in Alzheimer's disease (*18*), highlighting the important role of *APOE* in neurologic disorders. Furthermore, the role of *APOE* has been reported in atherosclerosis (*19*) and also in the pathogenesis of glaucoma (*20*). In addition, *APOE* also serves as a transcription factor that regulates gene expression, influencing lipid transport, inflammation, and cellular stress (*21*). In the context of inflammation and oxidative stress, *APOE*'s regulatory

[1]Beijing Institute of Ophthalmology, Beijing Tongren Hospital, Capital Medical University, Beijing 100730, China. [2]Department of Ophthalmology, Xuanwu Hospital, Capital Medical University, Beijing, China. [3]The First Affiliated Hospital of Chongqing Medical University, Chongqing Key Laboratory of Ophthalmology, Chongqing Eye Institute, Chongqing Branch (Municipality Division) of National Clinical Research Center for Ocular Diseases, Chongqing, China.
*Corresponding author. Email: sphou828@163.com (S.H.); dfylei@126.com (F.L.)
†These authors contributed equally to this work.

functions can modify the expression of genes that either mitigate or exacerbate these conditions (*22*, *23*). Nevertheless, little is known about the function of *APOE* in microglia in the pathogenesis of uveitis. Thus, studying *APOE* might provide new insights into uveitis pathology and therapy.

Reactive oxygen species (ROS), including superoxide and hydrogen peroxide, play a critical role in the inflammatory and autoimmune conditions. Predominantly generated in mitochondria, these molecules function as signaling agents that modulate immune responses, influencing the activation and proliferation of immune cells (*24*–*26*). Although essential for defending against pathogens, excessive ROS production results in oxidative stress, thereby exacerbating inflammation and tissue damage (*27*). In autoimmune diseases, excessive ROS also intensify chronic inflammation and injury (*28*).

Peptidyl prolyl isomerase F (*PPIF*), commonly referred to as *cyclophilin D*, is a pivotal mitochondrial matrix protein that facilitates protein folding and regulates the mitochondrial permeability transition pore (mPTP) (*29*). Dysregulation of *PPIF* is associated with elevated production of ROS and mitochondrial dysfunction (*30*). Recent studies have demonstrated a close association between *PPIF* and cardiovascular diseases (*31*), as well as its role in the regulation of hematopoietic stem cells (*32*). In the context of inflammation and autoimmune diseases, *PPIF* exacerbates tissue damage by promoting cell death and oxidative stress (*33*, *34*), and the interplay between *PPIF* and ROS intensifies inflammatory responses.

In this study, patients diagnosed with Vogt-Koyanagi-Harada (VKH) disease, a subgroup of AU, were enrolled; their peripheral blood mononuclear cells (PBMCs) were harvested for transcriptomic studies, and we identified significant enrichment of oxidative stress pathway components together with an up-regulated expression of *APOE* and its associated classical inflammatory signatures. In parallel, a murine model of EAU was used to investigate the transcriptome changes in microglia by single-cell RNA sequencing (RNA-seq), and up-regulation of *APOE* was also noted. Subsequent in vivo experiments using both wild-type (WT) and $APOE^{-/-}$ mice and in vitro cell assays established the positive correlation in *APOE* expression, microglial activation, and uveitis development. In addition, proteomic studies using mass spectrometry identified several downstream pathways in *APOE*-mediated microglial activation. In particular, ROS pathway was also highlighted and chosen for further analysis and PPIF protein was observed differentially expressed; moreover, high expression of *PPIF* was concurrently confirmed in samples from patients with VKH. Further research showed that the supplementation of *PPIF* reversed the disruption of microglial activation caused by *APOE* knockdown. Collectively, our data demonstrate that *APOE* is a key mediator in microglia activation and uveitis pathogenesis through *PPIF*, thereby expanding a comprehensive understanding of the uveitis pathophysiology as well as providing potential therapeutic strategies in uveitis.

RESULTS

Transcriptome of patients with VKH and single-cell RNA-seq of EAU murine retina revealed a pattern of high microglial expression of *APOE*

We performed transcriptomic profiling from PBMCs derived from patients with VKH and revealed a significant enrichment of pathways related to inflammation via gene ontology (GO) analysis (Fig. 1A). We observed prominent transcriptional up-regulation of classical inflammatory genes in patients with VKH (e.g., *CXCL2*, *JUN*, and *DUSP8*; Fig. 1B), with concurrent elevation in immune activity–related lipid metabolism genes (e.g., *CYP2A6*, *APOE*, and *SOSC3*; Fig. 1C). To investigate the transcriptomic differences in microglia between naïve and EAU mice, retinal immune cells defined as $CD45^+$ were fluorescence activated cell sorting (FACS) sorted and single-cell RNA-sequencing was performed after EAU immunization (Fig. 1D) (*35*). A significant increase in $CD45^+$ cells was observed in EAU mice (Fig. 1E), further clustering revealed that the majority of $CD45^+$ cells were microglia (Fig. 1F), and their relative abundance was markedly elevated in retinas of EAU mice (Fig. 1G). Furthermore, transcriptomic comparison between naïve and EAU microglia identified *APOE* as one of the top-listed differentially up-regulated genes (Fig. 1, H and I), which was also observed in the transcriptome of patients with VKH. Notably, violin plots demonstrated that microglia specific genes such as *P2ry12* (Fig. 1J) and *Tmem119* (Fig. 1K) were down-regulated in retinal microglia of EAU mice, whereas *APOE* expression was prominently up-regulated (Fig. 1L). Thus, the transcriptomic data suggested that high expression of *APOE* in retinal microglia under EAU immunization might play a critical role in determining its inflammatory phenotype.

Up-regulated *APOE* expression is positively associated with EAU-induced inflammation

To validate the discoveries from single-cell RNA-seq, EAU-induced mice were systematically evaluated from both pathologic and molecular aspects (*36*). EAU mice presented with severe ocular inflammation and abnormalities; under slit lamp iritis, anterior chamber turbidity and sclera vessel dilation could be observed (Fig. 2, A and B). Histologic examination of the posterior segment showed vitreous infiltration, retinitis, and choroiditis (Fig. 2, C and D). Further analysis of retinal protein profiles demonstrated that the expression of APOE and several inflammation-related proteins, including inducible nitric oxide synthase (iNOS), TNF-α, and IL-6, was up-regulated (Fig. 2, E to I). To further investigate the relationship between retinal APOE expression and microglia, immunofluorescent staining to IBA1 and APOE was performed, and it was found that under EAU immunization, APOE expression is significantly up-regulated in the retina and mainly by $IBA1^+$ microglia (Fig. 2, J and K). These data suggested that up-regulated APOE expression in the retina of EAU mice was mediated by microglia and positively associated with the degree of inflammation.

APOE is the key mediator in microglia-mediated EAU pathogenesis

To investigate the role of *APOE* in EAU pathogenesis, WT and $APOE^{-/-}$ mice were used. Consistent with the established association between *APOE*, microglial activation, and inflammation, $APOE^{-/-}$ mice markedly diminished EAU phenotype in both anterior (Fig. 2, L and M) and posterior segments (Fig. 2, N and O). Meanwhile, retinal tissues from $APOE^{-/-}$ mice showed the decreased expression of inflammation-related molecules, including iNOS, TNF-α, and IL-6 (Fig. 2, P to T). Meanwhile, flow cytometric analysis revealed that *APOE* knockout significantly reduced the inflammatory cytokines expressed by retinal microglia ($CD45^+CD11b^+CX3CR1^+$) in uveitis (fig. S1, A to G). To further investigate this, we constructed an adeno-associated viral vector to deliver *APOE*-shRNA (short hairpin RNA). Following intravitreal

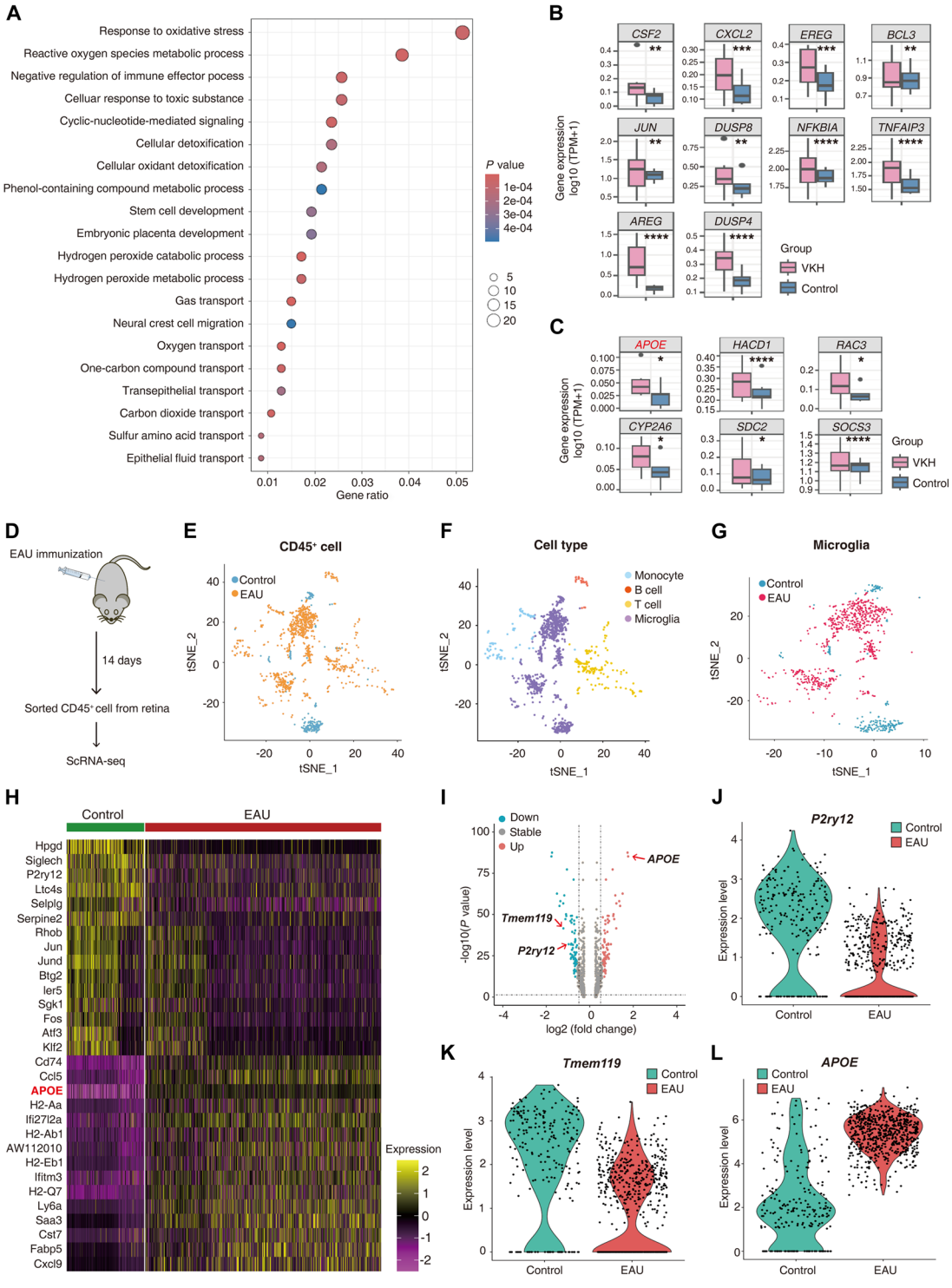

Fig. 1. The analysis of transcriptome of patients with VKH and single-cell RNA-seq of EAU murine retina. (**A**) GO analysis of transcriptome of patients with VKH. (**B**) Boxplot of signature differentially expressed genes related to inflammation from transcriptome of patients with VKH (statistical analysis: $^{**}P < 0.01$, $^{***}P < 0.001$, $^{****}P < 0.0001$). (**C**) Boxplot of signature differentially expressed genes in immune activity–related lipid metabolism from transcriptome of patients with VKH (statistical analysis: $^{*}P < 0.05$, $^{****}P < 0.0001$). (**D**) Schematic illustration of the murine experimental design of the single-cell transcriptomic sequencing. (**E**) Single-cell RNA-seq revealed the retinal CD45^{+} cell population from naïve and EAU mice. (**F**) Subclusters of CD45^{+} cells, including monocytes, B cells, T cells, and microglia. (**G**) t-SNE plot of the microglia isolated from both naïve and EAU retina. (**H**) Heatmap showing the differentially expressed gene in microglia between naïve and EAU mice. (**I**) Volcano plot showing the microglial gene expression patten in EAU mice compared to that of naïve mice; violin plots showing the differential expression of *P2ry12* (**J**), *Tmem119* (**K**), and *APOE* (**L**) between naïve and EAU mice.

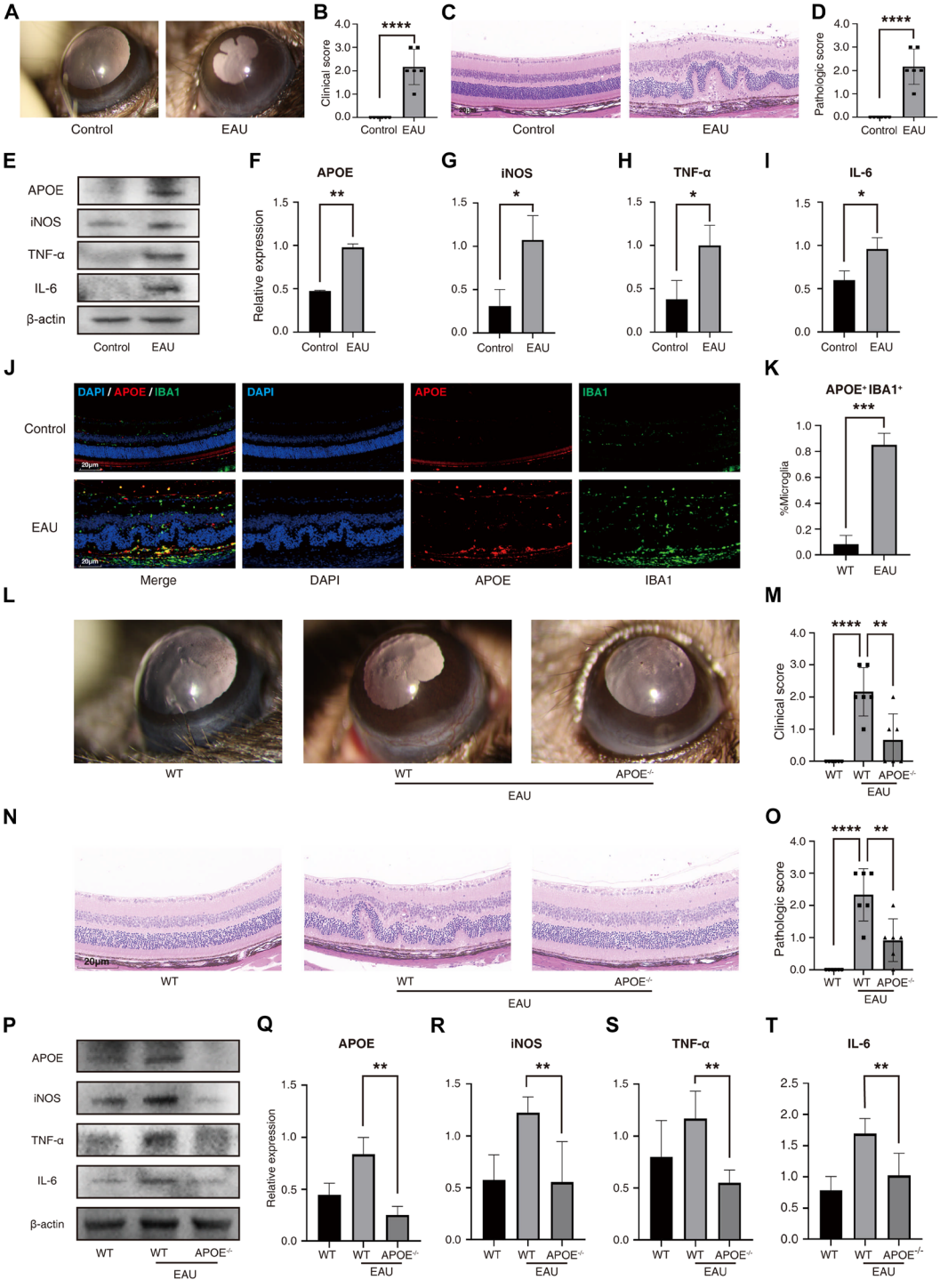

Fig. 2. Microglia modulate the inflammatory phenotype of EAU mice through the regulation of the key mediator *APOE*. (**A**) Slit lamp images showing the anterior segment from naïve and EAU mice. (**B**) Clinical scores of naïve and EAU mice (statistical analysis: mean ± SEM; $n = 6$ per group; $^{****}P < 0.0001$). (**C**) Histologic images of posterior segments of the eye from naïve and EAU mice. (**D**) Pathologic scores of naïve and EAU mice (statistical analysis: mean ± SEM; $n = 6$ per group; $^{****}P < 0.0001$). (**E**) Western blotting images showing the differential expression of different proteins. Image quantification of the differentially expressed proteins: APOE (**F**), iNOS (**G**), TNF-α (**H**), and IL-6 (**I**) (statistical analysis: mean ± SEM; $n = 3$ per group; $^{*}P < 0.05$, $^{**}P < 0.01$). (**J**) Immunofluorescent images showing the association of IBA1 and APOE. (**K**) quantification of $APOE^{+}$ $IBA1^{+}$ cells in naïve and EAU retina (statistical analysis: mean ± SEM; $n = 3$ per group; $^{***}P < 0.001$). (**L**) Slit lamp images showing the anterior segment from naïve WT, EAU-induced WT, and $APOE^{-/-}$ mice. (**M**) Clinical scores of different groups of mice (statistical analysis: mean ± SEM; $n = 6$ per group; $^{**}P < 0.01$, $^{****}P < 0.0001$). (**N**) Histologic images of posterior segments of the eye from naïve WT, EAU-induced WT, and $APOE^{-/-}$ mice. (**O**) Pathologic scores of different groups of mice (statistical analysis: mean ± SEM; $n = 6$ per group; $^{**}P < 0.01$, $^{****}P < 0.0001$). (**P**) Western blotting images showing the differential expression. Image quantification of the differentially expressed proteins: APOE (**Q**), iNOS (**R**), TNF-α (**S**), and IL-6 (**T**) (statistical analysis: mean ± SEM; $n = 3$ per group; $^{**}P < 0.01$).

injection of the adeno-associated virus, EAU was induced. The results demonstrated that the knockdown of *APOE* significantly ameliorated disease severity, thereby identifying *APOE* as a key molecular driver of uveitis pathogenesis (fig. S2, A to D). These findings supported the critical role of *APOE* in retinal inflammation of EAU immunization mice.

Microglial expression of *APOE* is inflammation dependent

An in vitro microglial activation model was used to investigate the relationship between APOE expression and the cascade of inflammation (*37*). In brief, human microglia cell line HMC3 was used and stimulated with different concentrations of IL-17a and interferon-γ (IFN-γ), which was a well-characterized cytokine combination for inducing proinflammatory microglial responses (*38*–*40*). It was found that the degree of inflammation as well as APOE expression in HMC3 cells was positively associated with the concentration of stimulation. The stimulation by higher concentrations of IL-17a and IFN-γ up-regulated APOE, iNOS, TNF-α, and IL-6 expression (Fig. 3, A to E). Migration assay showed that the migratory capability of HMC3 cells was also associated with the strength of stimulation (Fig. 3, F and G). Meanwhile, the 5-ethynyl-2′-deoxyuridine (EdU) incorporation assay showed that the proliferation capability of HMC3 cells was also enhanced in accordance with the degree of inflammation (Fig. 3, H and I). These data indicated that *APOE* was tightly associated with the inflammatory phenotype and severity of the microglia.

Disruption of *APOE* ameliorates microglial inflammation through *PPIF*

As mentioned above, *APOE* mediated microglial inflammation, and thus, it was interesting to evaluate whether knockdown of *APOE* in microglia could reduce the inflammation. To knock down *APOE*, a lentiviral delivery system was used. shRNA targeting *APOE* (sh-*APOE*) was cloned into a green fluorescent protein (GFP)-tagged lentiviral vector to mediate the gene transduction (Fig. 3J). Following lentiviral transduction, HMC3 cells were stimulated with IL-17a and IFN-γ before harvesting for protein analysis. We found that *APOE* knockdown diminished the expression of inflammatory mediators iNOS, TNF-α, and IL-6 as described above (Fig. 3, K to O). In addition, *APOE* knockdown also diminished expedited cell migration (Fig. 3, P and Q) and cell proliferation (Fig. 3, R and S) after receiving IL-17a and IFN-γ stimulation. To elucidate the mechanism involved in *APOE*-mediated activation of microglial inflammation, proteomic analysis was performed to cytokine-stimulated HMC3 cells with or without *APOE* knockdown (Fig. 4A). Kyoto Encyclopedia of Genes and Genomes (KEGG) pathway analysis revealed that oxidative phosphorylation and ROS pathways were highly up-regulated in stimulated HMC3 cells compared to unstimulated cells, but remained repressed in stimulated *APOE* knockdown cells (Fig. 4, B and C). Further analysis of the two above mentioned pathways identified *PPIF* as a potential downstream regulator of *APOE* pathway in microglia (Fig. 4D). Notably, elevated expression of oxidative stress–associated genes including *PPIF* was also identified in patients with VKH (Fig. 4E). To further verify the expression, we performed Western blot analysis, which validated that PPIF was a downstream component of APOE (Fig. 4, F to H). In summary, these datasets supported the critical role of *APOE* in regulating microglial inflammation and suggested that *APOE* regulated microglial inflammation through *PPIF*.

Supplementation of *PPIF* reverses *APOE* deficiency–caused impaired ROS expression

To further validate whether *PPIF* is a true downstream mediator of the *APOE* pathway, a red fluorescent protein (RFP)–tagged lentiviral vector overexpressing *PPIF* was generated and delivered gene into *APOE* knockdown HMC3 cells. The experimental design was depicted in Fig. 5A, and the efficiency of dual transduction of both empty and gene-loaded lentiviral vectors was documented in Fig. 5B. Results showed that supplementation of *PPIF* to *APOE* knockdown cells partially reversed the impaired ROS expression as iNOS expression was restored (Fig. 5, C to F). We also analyzed ROS expression changes in microglia and found that *PPIF* supplementation effectively reversed the impaired ROS expression induced by *APOE* intervention in microglia (Fig. 5, G and H). Furthermore, we observed that *PPIF* supplementation in *APOE* knockdown HMC3 cells did not alter the mitochondrial basal oxygen consumption rate (OCR), but significantly reduced ATP coupling efficiency and reversed proton leakage compared to *APOE* knockdown HMC3 cells (Fig. 5, I to L). Both mitochondrial proton leak and the aberrant mPTP opening mediated by *PPIF* up-regulation are closely associated with ROS production (*41*, *42*). Thus, our findings demonstrated that microglia regulated *PPIF* expression through *APOE*-dependent signaling, which subsequently modulated ROS production.

APOE modulates ROS expression through *PPIF* in mouse model of EAU

Moreover, adenovirus was injected into the vitreous cavity of WT mice and *APOE* KO mice to overexpress *PPIF* in the retina, followed by EAU immunization 2 weeks later. Subsequently, we observed that the *PPIF* overexpression failed to reverse the suppression of EAU development caused by *APOE* knockout, suggesting the pleiotropic functions of *APOE* in EAU pathology (Fig. 6, A to D). Further analysis of retinal protein revealed that *PPIF* overexpression reversed ROS dysregulation caused by *APOE* gene knockout as the reversal of iNOS levels in EAU mice compared to *APOE* KO mice (Fig. 6, E to H). Flow cytometric analysis of retinal microglia in this model revealed that *PPIF* supplementation could not fully reverse the attenuated inflammatory phenotype in $APOE^{-/-}$ mice (fig. S3, A to D). In addition, to further verify the role of *PPIF* in EAU mice, adenovirus was injected into the vitreous cavity of WT mice to overexpress *PPIF* in the retina, followed by EAU immunization 2 weeks later. The results showed the overexpression of *PPIF* exacerbated retinal pathological changes under EAU immunization (Fig. 6, I to L). Further analysis of retinal microglia revealed that *PPIF* overexpression up-regulated the expression of inflammatory cytokines, including TNF-α, IL-6, and iNOS (fig. S4, A to F). Together, these findings indicate that *PPIF* might function as an important factor influencing the progression of uveitis.

DISCUSSION

Microglia play a crucial role in the pathogenesis of various types of neurological diseases, including neuroinflammatory, autoimmune, and degenerative diseases (*43*). Substantial evidence has demonstrated that microglia are essential not only for maintaining homeostasis in CNS but also for modulating inflammation (*44*, *45*). Dysregulated microglial activation leads to the release of numerous proinflammatory mediators, thus further exacerbating the progression of various inflammatory diseases (*46*). Studies suggest that

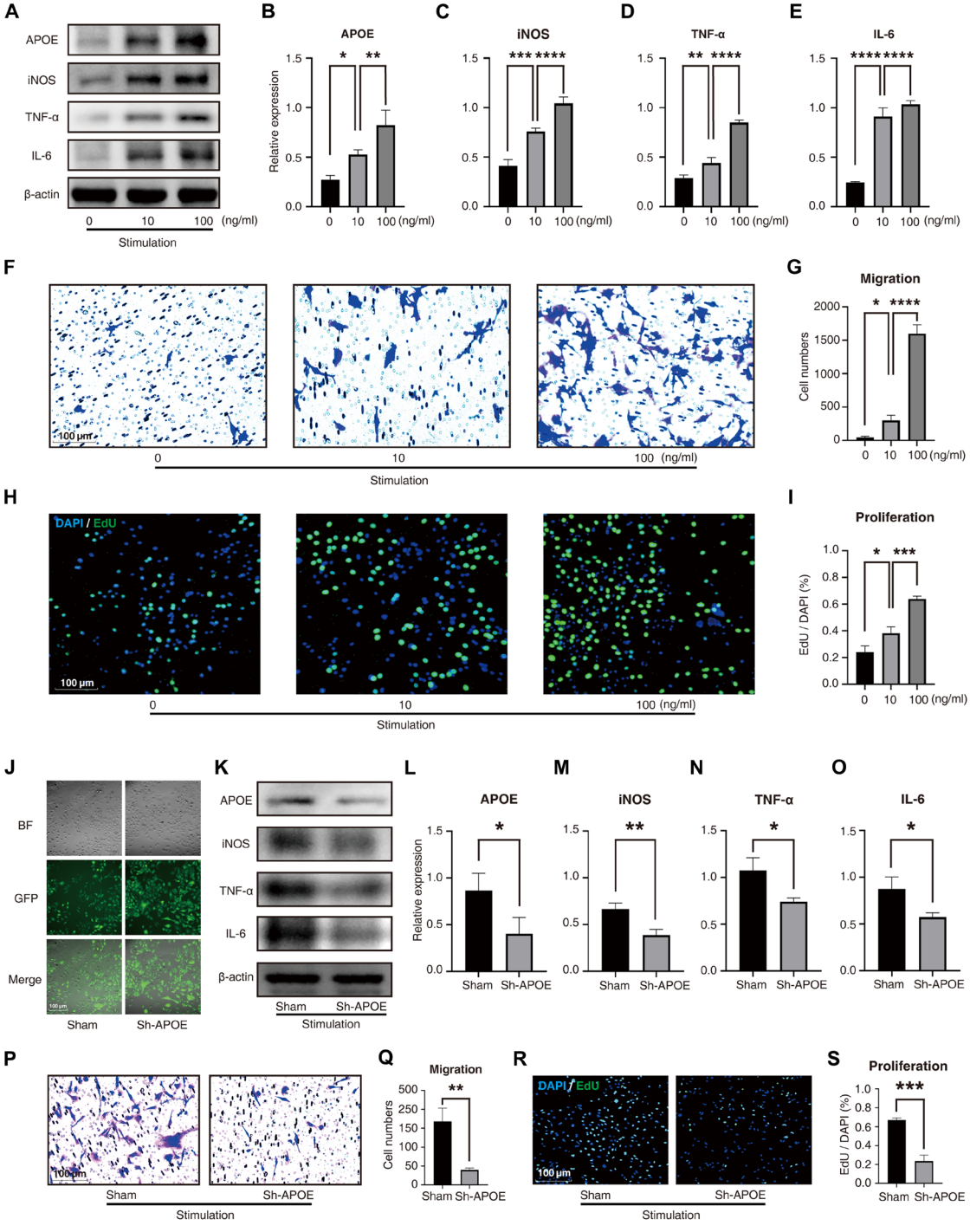

Fig. 3. *APOE* is a pivotal gene regulating the inflammatory phenotype of microglia. (**A**) Western blotting images showing the protein expressions of iNOS, APOE, TNF-α, IL-6, and β-actin in HMC3 cells after in vitro stimulation with different concentrations of IL-17a and IFN-γ. Image quantification of the differentially expressed proteins: APOE (**B**), iNOS (**C**), TNF-α (**D**), and IL-6 (**E**) (statistical analysis: mean ± SEM; $n = 3$ per group; $^{*}P < 0.05$, $^{**}P < 0.01$, $^{***}P < 0.001$, $^{****}P < 0.0001$). (**F**) Migration assay showing the mobility of HMC3 cells under the stimulation of different concentration of cytokines. (**G**) Quantification of migrated HMC3 cells (statistical analysis: mean ± SEM; $n = 3$ per group; $^{*}P < 0.05$, $^{****}P < 0.0001$). (**H**) EdU incorporation assay showing the proliferation of HMC3 cells under the stimulation of different concentration of cytokines. (**I**) Quantification of EdU^{+} HMC3 cells (statistical analysis: mean ± SEM; $n = 3$ per group; $^{*}P < 0.05$, $^{***}P < 0.001$). (**J**) GFP expression in HMC3 cells transduced by GFP-tagged sham or sh-*APOE* lentiviral vector. (**K**) Western blotting images showing the protein expressions of APOE, iNOS, TNF-α, IL-6, and β-actin in lentivirally transduced HMC3 cells. Image quantification of the differentially expressed proteins: APOE (**L**), iNOS (**M**), TNF-α (**N**), and IL-6 (**O**) (statistical analysis: mean ± SEM; $n = 3$ per group; $^{*}P < 0.05$, $^{**}P < 0.01$). (**P**) Migration assay showing the mobility of lentivirally transduced HMC3 cells under cytokine stimulation. (**Q**) Quantification of migrated HMC3 cells (statistical analysis: mean ± SEM; $n = 3$ per group; $^{**}P < 0.01$). (**R**) EdU incorporation assay showing the proliferation of lentivirally transduced HMC3 cells under cytokine stimulation. (**S**) Quantification of EDU^{+} HMC3 cells (statistical analysis: mean ± SEM; $n = 3$ per group; $^{***}P < 0.001$).

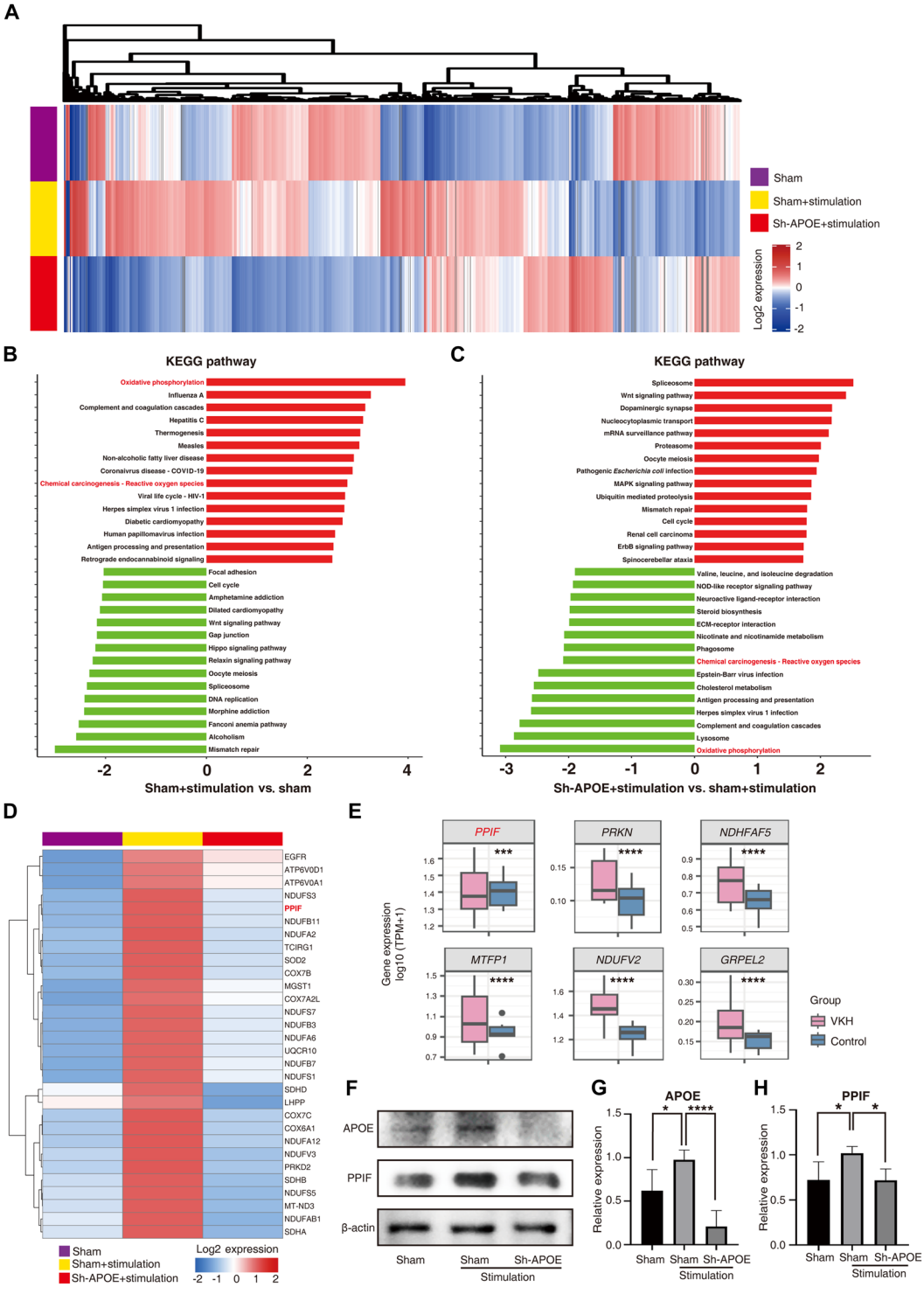

Fig. 4. Proteomic profiling of HMC3 cells. (**A**) Heatmap of protein expression in different groups of HMC3 cells. Sham: HMC3 cell transduced with empty lentiviral vector; stimulation: HMC3 cells stimulated with IL-17a and IFN-γ; Sh-*APOE*: HMC3 cells transduced with lentiviral vector expressing *APOE* short-hairpin RNA to knock down *APOE*. (**B**) KEGG pathway analysis comparing the proteomic profile of stimulated HMC3 cells to that of unstimulated HMC3 cells. (**C**) KEGG pathway analysis comparing the proteomic profile of stimulated, *APOE* knocked-down HMC3 cells to that of stimulated HMC3 cells. (**D**) Heatmap protein expression profiles of those in the ROS pathway. (**E**) Heatmap of signature differentially expressed genes related to ROS pathways from transcriptome of patients with VKH. (**F**) Western blotting images showing the protein expressions of APOE, PPIF, and β-actin in different groups of HMC3 cells. Image quantification of the differentially expressed proteins: APOE (**G**) and PPIF (**H**) (statistical analysis: mean ± SEM; $n = 3$ per group; $^{*}P < 0.05$, $^{****}P < 0.0001$).

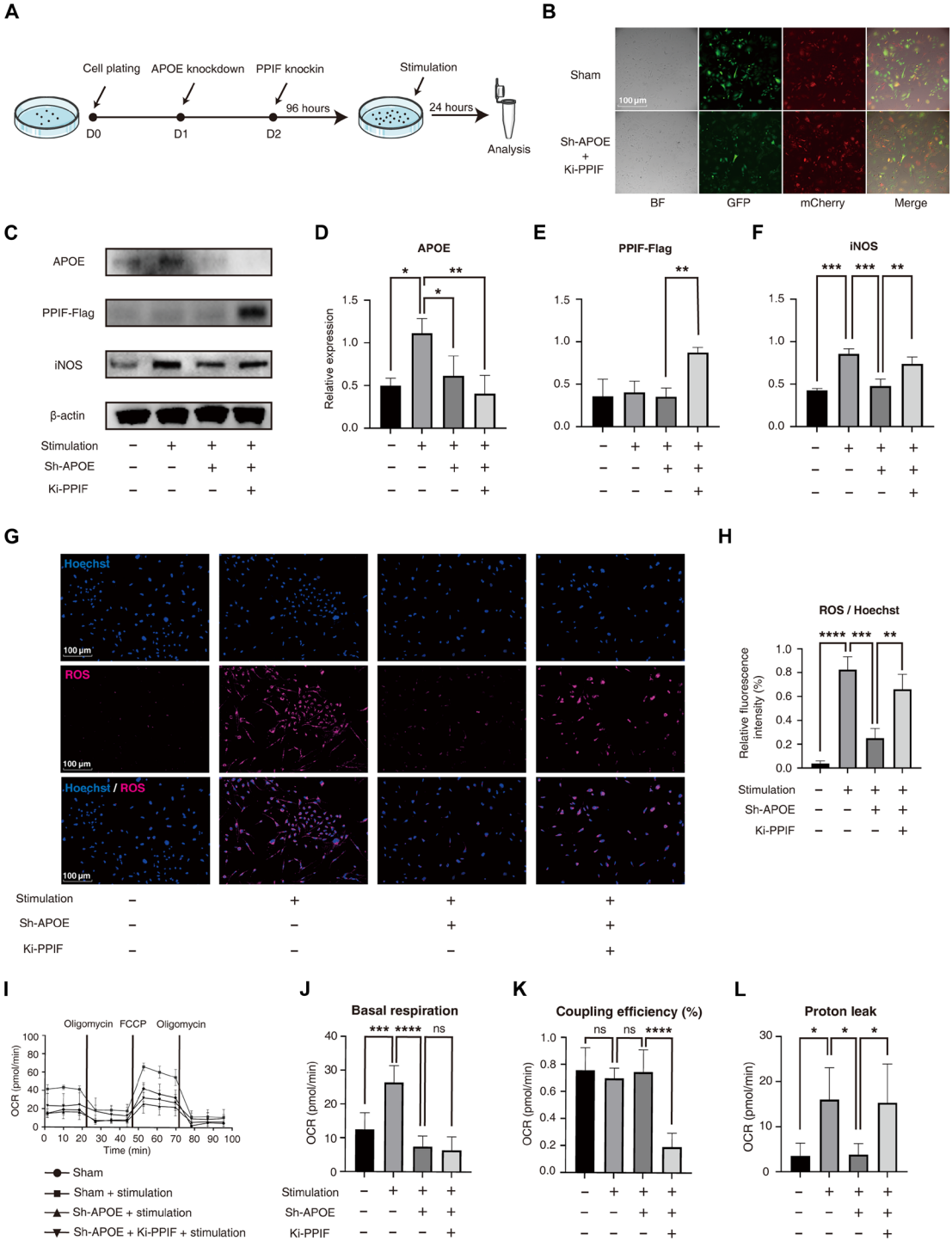

Fig. 5. Supplementation of *PPIF* reverses *APOE* deficiency–caused impaired ROS expression and causes mitochondrial function alterations. (**A**) Schematic illustration of the experimental design. (**B**) Fluorescent images of lentiviral transduced HMC3 cells. Lentiviral vectors are tagged with either GFP (*APOE* knockdown, Sh-*APOE*) or RFP (*PPIF* knock in, Ki-*PPIF*) to visualize the gene transduction. (**C**) Western blotting images showing the protein expressions of APOE, PPIF, iNOS, and β-actin in different groups of HMC3 cells. Image quantification of the differentially expressed proteins: APOE (**D**), PPIF (**E**), and iNOS (**F**) (statistical analysis: mean ± SEM; $n = 3$ per group; $^{*}P < 0.05$, $^{**}P < 0.01$, $^{***}P < 0.001$). (**G**) Fluorescence microscopy reveals alterations in ROS levels following *PPIF* supplementation in *APOE* knockdown HMC3 cells. (**H**) Statistical analysis of the relative fluorescence intensity of ROS (statistical analysis: mean ± SEM; $n = 3$ per group; $^{**}P < 0.01$, $^{***}P < 0.001$, $^{****}P < 0.0001$). (**I**) Oxygen consumption rate (OCR) in microglia are measured using a Seahorse analyzer. (**J**) Comparison of basal mitochondrial respiration across different microglial groups (statistical analysis: mean ± SEM; $n = 5$ per group; $^{***}P < 0.001$, $^{****}P < 0.0001$). (**K**) Comparison of ATP coupling efficiency across different microglial groups (statistical analysis: mean ± SEM; $n = 5$ per group; $^{****}P < 0.0001$). (**L**) Comparison of proton leak across different microglial groups (statistical analysis: mean ± SEM; $n = 5$ per group; $^{*}P < 0.05$).

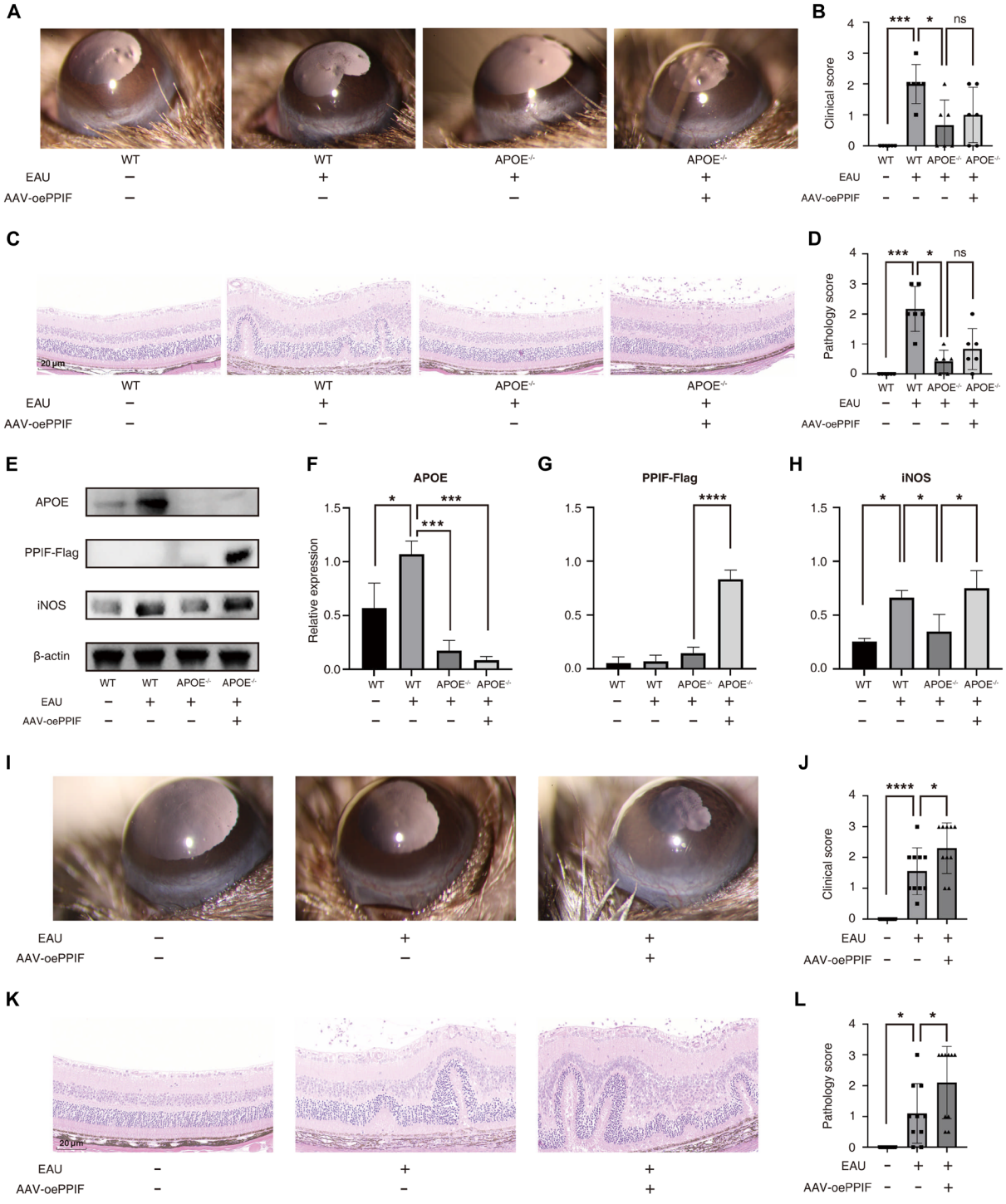

Fig. 6. Supplementation of *PPIF* reverses the impaired ROS expression caused by *APOE* gene knockout in EAU mice. (**A**) Slit lamp images showing the anterior segment from naïve WT, EAU-induced WT or *APOE*$^{-/-}$ mice, and EAU-induced *APOE*$^{-/-}$ mice after adenovirus intravitreal injection. (**B**) Clinical scores of different groups of mice (statistical analysis: mean ± SEM; $n = 6$ per group; $^{*}P < 0.05$, $^{***}P < 0.001$). (**C**) Histologic images of posterior segments of the eye from naïve WT, EAU-induced WT or *APOE*$^{-/-}$ mice, and EAU-induced *APOE*$^{-/-}$ mice after adenovirus intravitreal injection. (**D**) Pathologic scores of different groups of mice (statistical analysis: mean ± SEM; $n = 6$ per group; $^{*}P < 0.05$, $^{***}P < 0.001$). (**E**) Western blotting images showing the protein expressions of APOE, PPIF, iNOS, and β-actin in retinal lysates from different group of mice. Image quantification of the differentially expressed proteins: APOE (**F**), PPIF (**G**), and iNOS (**H**) (statistical analysis: mean ± SEM; $n = 3$ per group; $^{*}P < 0.05$, $^{***}P < 0.001$, $^{****}P < 0.0001$). (**I**) Slit lamp images showing the anterior segment from naïve WT, EAU-induced WT, and EAU-induced WT after adenovirus intravitreal injection. (**J**) Clinical scores of different groups of mice (statistical analysis: mean ± SEM; $n = 10$ per group; $^{*}P < 0.05$, $^{****}P < 0.0001$). (**K**) Histologic images of posterior segments of the eye from naïve WT, EAU-induced WT, and EAU-induced WT after adenovirus intravitreal injection. (**L**) Pathologic scores of different groups of mice. (statistical analysis: mean ± SEM; $n = 10$ per group; $^{*}P < 0.05$).

microglia have an indispensable role in the pathology of uveitis (*47*), and microglia depletion by using a small-molecule CSF1R inhibitor could alleviate the pathology and severity of EAU mice, although the CSF1R inhibitor PLX5622 has been reported to have side effects targeting microglia; other microglia depletion approaches such as using genetic ablation further validate this finding (*48*). Microglia exhibit diverse functions, including proinflammatory, anti-inflammatory, and reparative roles (*49*). Consequently, the role of microglia in uveitis requires detailed analysis.

In exploring the proinflammatory properties of microglia, we performed single-cell RNA-seq of retinal immune cells at the peak of murine uveitis and identified elevated *APOE* expression in activated microglia. *APOE* is a glycoprotein that is widely expressed in various cell types within the CNS, including astrocytes, microglia, vascular wall cells, and choroid plexus cells (*50*). It plays a pivotal role in numerous biological processes, including immune regulation (*51*), inflammation (*52*), and metabolism (*53*). Furthermore, *APOE* also functions as a transcription factor, intricately regulating gene expression and participating in the progression of disease (*54*, *55*). Its involvement in inflammatory pathways necessitates more comprehensive investigation to understand its specific role and mechanism in various contexts.

Previous studies have predominantly focused on elucidating the association between *APOE* and Alzheimer's disease (*56*). In this study, we observed elevated *APOE* expression in microglia after EAU immunization, which has not been reported. We found that targeting *APOE* significantly suppressed the activation of microglia and ameliorated the severity of EAU mice, highlighting *APOE* as a critical regulator of EAU initiation and progression.

To elucidate the specific mechanisms for how *APOE* modulates microglia-involved pathogenesis of uveitis, we performed proteomic analysis of the in vitro stimulated human microglia cell line HMC3 to investigate the proteomic changes and potentially involved pathways (*57*). Subsequently, we identified a strong association between *APOE* and the ROS family in the EAU development, with a particular emphasis on the *PPIF* gene. Emerging evidence indicates that *APOE* plays a key role in regulating mitochondrial function (*58*). *PPIF*—a central modulator of mPTP (*59*)—also plays a significant role in regulating ROS production (*60*) and lipid metabolism (*61*). Recent studies have demonstrated a pivotal interaction between endothelial nitric oxide synthase and S-nitrosylated *PPIF* in *APOE* knockout mice, and similarly, several other investigations have suggested the critical role of *PPIF* in the pathogenesis of atherosclerosis in *APOE* knockout mice (*62*, *63*). These findings collectively highlight the intricate relationship between *APOE* and *PPIF*. Notably, both *APOE* and *PPIF* exhibited differential expression patterns in transcriptomic sequencing of clinical patient-derived specimens. In conclusion, our research elucidated a previously unknown signaling pathway in uveitis, wherein microglia regulated the expression of *PPIF* genes within the ROS family through *APOE*, thereby modulating ROS expression.

Although we provided a complete study describing the mechanism of microglia activation in the pathogenesis of uveitis, several limitations still exist, the first of which is the use of the microglia cell line HMC3 and in vitro stimulation. It does not fully recapitulate the in vivo retinal microenvironment; however, in terms of inflammatory response, it could serve as a usable model. In vivo studies would require a large cohort of animals to obtain adequate number of retinal microglia cells for proteomic analysis. Thus, an in vitro model is a reasonable substitute. Second, for immunoblotting of PPIF, FLAG was used to better distinguish exogenous PPIF from endogenous PPIF, as *PPIF* is a key molecule in maintaining mitochondrial function, and knockdown of *APOE* might not fully eliminate endogenous PPIF as mitochondria structural components. While the systemic knockout of *APOE* in mice does not significantly affect inflammatory processes in other retinal immune cells, including T cells, dendritic cells, astrocytes, Müller cells, and retinal pigment epithelial cells (*64*–*68*), *APOE* plays a critical role as a transcription factor in microglial physiology, and the lack of it significantly abolishes microglial activation as well as uveitis development. Moreover, *APOE* is a highly multifunctional molecule that participates in various biological processes including lipid metabolism, mitochondrial function, immune regulation, and neurodegenerative processes (*69*). Therefore, supplementation with *PPIF* might not fully reverse the disrupted microglial inflammation. It might cause the bioinformatic analysis of the proteomic data to limit the complete description of *APOE*-regulated microglial function, and this could be overcome by combining proteomic analysis together with transcriptomic and/or epigenetic analysis. In summary, this study describes the role of *PPIF* in *APOE*-regulated microglial activation and following uveitis development.

MATERIALS AND METHODS

Patient diagnosis and specimen processing

Researchers randomly collected whole-blood specimens from six patients with VKH and six age-matched healthy controls at Beijing Tongren Hospital. All VKH cases fulfilled international diagnostic criteria (*70*) with the exclusion of ocular trauma or intraocular surgical history. The study protocol was approved by the Institutional Review Board of Beijing Tongren Hospital (protocol no. TREC2024-KY106) in compliance with the Declaration of Helsinki. Written informed consent was obtained from patients before enrollment.

Whole-blood specimen RNA-seq

High pure RNA was extracted from PBMCs following the protocol of the TRNzol Universal Reagent Kit (TIANGEN Biotech, stock no. DP424). Sequencing libraries were generated using the VAHTS Universal V8 RNA-seq Library Prep Kit for Illumin (Vazyme) following the manufacturer's recommendations, and index codes were added to attribute sequences to each sample. The sequencing libraries were quantified using the Invitrogen high-sensitivity DNA assay on Qubit 4.0, and the integrity was detected with the Agilent Bioanalyzer 2100 system. Then, the sequencing library was sequenced on the MGISEQ-T7 platform and 150-bp paired-end reads were generated.

Animals

All animal-related experimentations were conducted in accordance with the Association for Research in Vision and Ophthalmology Statement for the Use of Animals in Ophthalmic and Vision Research and the NIH's *Guide for the Care and Use of Laboratory Animals*. Animal research protocol approval was obtained at the Beijing Tongren Hospital, Capital Medical University (protocol no. TRLAWEC2024-03). Six- to eight-week-old C57BL/6NCrl mice (stock no. 027) were obtained from Charles River Laboratories (Beijing, China), and $APOE^{-/-}$ (stock no. C001067) mice were obtained from Cyagen Biosciences (Suzhou, China). Mice were regularly housed at the animal facility at Beijing Institute

of Ophthalmology, Beijing Tongren Hospital affiliated to Capital Medical University.

EAU induction

EAU was induced as described previously. The human $IRBP_{651–670}$ peptide (LAQGAYRTAVDLESLASQLT, Sangon) was dissolved in sterile phosphate-buffered saline (PBS) and subsequently mixed with equal volume of complete Freund's adjuvant (Sigma-Aldrich, stock no. F5881) (*10*). Emulsification was obtained by using manual mixing in ice-chilled syringes. Emulsified $IRBP_{651–670}$ (500 μg) were injected subcutaneously together with 1 μg of pertussis toxin intraperitoneally (Sigma-Aldrich, stock no. P7208). All immunized mice were evaluated under a slit lamp 14 days after the injection to ensure the successful establishment of EAU. Both clinical and histopathological assessments were blindly scored by two individuals to validate the results (*71*).

Adenovirus intravitreal injection

Adenovirus for gene transductions was constructed, packaged, and purified by Shanghai Genechem Co. Ltd. In general, the *PPIF* gene was cloned into pAD-CAG-3FLAG-PPIF-P2A-mCherry-WPRE vector to deliver *PPIF*. 293T cells cotransfected with pCMV-dR8.91, pCMVVSV-G6363, and targeting vector were used to generate pseudoviral particles. *APOE* shRNA was cloned into PAAV-CAG-EGFP-mir30-arm-shRNA-WPRE vector 293T cells cotransfected with pHelper plasmid, RC8(AAV-8) plasmid, and targeting vector. Pseudoviral particles were then concentrated and purified by ultracentrifugation and titered before use.

Intravitreal injection was performed as described in the literature (*72*). In brief, following systemic and ocular surface anesthesia, as well as pupil dilation in mice, a precise volume of adenovirus was carefully injected into the vitreous cavity using a micro syringe, and EAU immunization was subsequently conducted 2 weeks later.

Slit lamp examination

For anterior segment evaluation, a slit lamp biomicroscope with an integrated high-resolution digital camera was used (Model SLM-8E, S & T Co. Ltd., Chongqing, China). Mice were manually immobilized, and eyes were gently exposed. Topical 0.5% proparacaine hydrochloride was applied for corneal anesthesia. Images were captured in a darkened room to reduce glare, with camera settings optimized for resolution and exposure. For EAU scoring, 0: no evident sign of inflammation; 1: mild ciliary hyperemia; 2: marked ciliary hyperemia; 3: severe ciliary hyperemia with iris synechiae; and 4: ocular atrophy or blindness.

Cell lines and cell culture

The human microglia cell line HMC3 was purchased from Procell (Wuhan, China). HMC3 cells were routinely cultured in minimum essential medium (BasalMedia, China) supplemented with 10% fetal bovine serum (Gibco, Australia) and 1% penicillin-streptomycin (Thermo Fisher Scientific) at 37°C in 5% CO_2.

Lentivirus transduction

Lentivirus for gene transductions was constructed, packaged, and purified by Shanghai Genechem Co. Ltd. In general, the *APOE* shRNA sequence was cloned into pMagic7.1-Puro/GFP vector, or the *PPIF* gene was cloned into pLVX-CMV-3FLAG-PPIF-CAG-mCherry-T2A-neomycin-WPRE vector to deliver either *APOE* shRNA or *PPIF*. 293T cells cotransfected with pCMV-dR8.91, pCMV-VSV-G6363, and targeting vector were used to generate pseudoviral particles. Pseudoviral particles were then concentrated and purified by ultracentrifugation and titered before use.

For retroviral transduction, in brief, HMC3 cells were seeded on a six-well plate with a density of 2×10^5 per well for 24 hours and then transduced with lentiviral vector to knock down *APOE* or knock in *PPIF*. After 72 hours, the efficiency of lentiviral transduction was evaluated using a fluorescence microscope (Leica DMi8, Germany). Lentiviral transduced cells were puromycin and neomycin selected for 2 days, and surviving cells were used for future experiments.

Hematoxylin and eosin staining

Eyes were surgically removed after euthanasia and immediately fixed with Eyeball Fixation Solution (Servicebio, Wuhan, Chian; stock no. G1109) for at least 24 hours, and then tissues were embedded in paraffin and sectioned at a thickness of 4 to 6 μm. Hematoxylin and eosin staining was performed on tissue sections per the manufacturer's instruction (Servicebio, Wuhan, China; stock no. G1005). For pathologic scoring, 0 points: no cellular infiltration, no structural changes; 0.5: mild cellular infiltration, no structural changes; 1: moderate cellular infiltration, mild focal retinal folds; 2: moderate cellular infiltration, marked retinal folds with focal photoreceptor cell damage; 3: severe cellular infiltration, extensive retinal folds accompanied by detachment, serous exudation, and subretinal hemorrhage, moderate photoreceptor cell damage; and 4: severe (or mild) cellular infiltration, retinal layer atrophy, extensive photoreceptor cell damage.

EdU incorporation assay

The proliferation of HMC3 cells was evaluated using an EdU incorporation assay with an EdU Cell Proliferation Kit (Beyotime, C0071S) in accordance with the manufacturer's instructions, and the number of EdU^+ cells was quantified using ImageJ software (NIH, Bethesda, MD).

Migration assay

A total of 1×10^4 HMC3 cells were seeded into the upper 8-μm pore size filter's chamber of 24-well Transwell (Corning, 3422) without fetal bovine serum, and an appropriate amount of medium containing fetal bovine serum was added into the lower chamber. After 24 hours, cells were fixed with 4% paraformaldehyde (Servicebio, Wuhan, Chian; stock no. G1101) and stained with 1% crystal violet (Servicebio, Wuhan, Chian; stock no. G1014). Then, the migrated cells were imaged using a fluorescent microscope (Leica DMi8, Germany), and the number of migrated cells was quantified using ImageJ software (NIH, Bethesda, MD).

Western blotting

Retinas were surgically retrieved and cells were trypsinized to generate lysates for Western blotting. In brief, tissues and cells were lysed and prepared using radioimmunoprecipitation assay lysis buffer (Beyotime, P0013B). Western blotting was performed as previously described (*73*). The primary antibodies used for Western blotting were as follows: Anti-iNOS (Cell Signaling Technology, 2982, diluted 1:1000); APOE (Cell Signaling Technology, 49285, diluted 1:1000); IL-6 (Proteintech, 21865-1-AP, diluted 1:1000; Cell Signaling Technology, 12912T, diluted 1:1000); TNF-α (Proteintech,

26405-1-AP, diluted 1:1000); PPIF (Proteintech, 18466-1-AP, diluted 1:1000); Anti-Flag (Cell Signaling Technology, 14793, diluted 1:1000); and Anti–β-actin (Proteintech, 81115-1-RR, diluted 1:5000). The secondary antibody used was Horseradish peroxidase (HRP)-conjugated Goat Anti-Rabbit IgG(H + L) (Proteintech, SA00001-2, diluted 1:5000). The ECL kit (Advansta, CA, USA) was used for protein blotting visualization. ImageJ software was used to analyze the blot images.

Immunofluorescence microscopy

The tissue paraffin sections were dewaxed, antigen retrieved, and blocked with 3% bovine serum albumin for 30 min and then incubated with primary antibody (anti-APOE, Servicebio, GB112288, 1:200; anti-IBA1, Wako, 019-19741-20, 1:3000) in a wet box at 4°C overnight. Then, the samples were incubated with different secondary antibodies at room temperature for 1 hour. Stained slides were sealed with 4′,6-diamidino-2-phenylindole (DAPI) mounting medium (Abcam, AB104139). Images were taken with a fluorescent microscope (Leica DMi8, Germany) and quantified using ImageJ software.

ROS detection

The culture medium was replaced after processing the cells, followed by the addition of the CellROX probe (Thermo Fisher Scientific, C10422) and the NucBlue Live Cell Stain ReadyProbes reagent (Thermo Fisher Scientific, R37605). The cells were subsequently incubated at a 37°C cell culture incubator for 30 min. After incubation, the cells were washed three times with PBS and observed under a fluorescence microscope (Leica DMi8, Germany).

OCR measurement

The cellular OCR was measured using the Seahorse XF Cell Mito Stress Test Kit (Agilent, Santa Clara, CA, USA) with the Seahorse XFe 24 Extracellular Flux Analyzer (Agilent), according to the manufacturer's protocol. In brief, 2.5×10^4 cells were seeded into a Seahorse XF 24 cell culture microplate per well. After recording baseline measurements, 1.5 μM oligomycin, 1.5 μM FCCP, and 1.0 μM rotenone–antimycin A were sequentially injected. Data were analyzed using the Seahorse Wave 2.6.3 software package (Agilent), and OCR values were expressed in picomoles per minute.

Flow cytometric analysis

Murine retinas were gently isolated and digested with a prepared papain dissociation system (Worthington, WK-LK003150) at 37°C for 20 min. The digested retinal tissue was then resuspended in PBS. For surface receptor staining, the prepared cell suspension was treated with a mouse Fc receptor blocking agent (Miltenyi Biotec, 130-092-575, diluted 1:100) and incubated at 4°C for 20 min, followed by staining with specific antibodies at 4°C in the dark for 20 min. Cells were then fixed and permeabilized using a flow cytometry fixation/permeabilization buffer (Thermo Fisher Scientific, 00-5223-56 and 00-5123-43) at room temperature in the dark for 10 min. For intracellular cytokine staining, the cells were subsequently incubated with a flow cytometry permeabilization buffer (Thermo Fisher Scientific, 00-8333-56), followed by the addition of specific antibodies and incubation at room temperature in the dark for 20 min. Acquisition and compensation were performed by Cytek Aurora Spectral Flow Cytometry. Data were exported and analyzed using FlowJo software (v10.9). Gating strategies are shown in figs. S2 to S4, and the antibodies used for flow cytometry were as follows: Anti-CD45 APC/Cyanine7 (BioLegend, 157204, diluted 1:100); Anti-CD11b Horizon RB705 (BD, 570292, diluted 1:100); Anti-CX3CR1 Pacific Blue (BioLegend, 149038, diluted 1:100); Anti–TNF-α Percp/Cyanine5.5 (BioLegend, 506322, diluted 1:50); Anti–IL-6 APC (BioLegend, 504508, diluted 1:50); and Anti-iNOS PE (BioLegend, 696806, diluted 1:50).

Proteomic analysis

Proteomic analysis was performed by Jingjie PTM Biolabs (Hangzhou, China). Briefly, HMC3 cells were harvested and lysed, and protein was extracted and hydrolyzed by trypsin. Subsequently, the peptide segments are dissolved in liquid chromatography mobile phase A and separated using the EASY-nLC 1200 ultrahigh-performance liquid phase system (Thermo Fisher Scientific). The peptide segments were analyzed by Orbitrap Exploris 480 mass spectrometry. Bioinformatic analysis was conducted with the assistance from Jingjie PTM Biolabs (Hangzhou, China). The DIA-NN search engine (v.1.8) was used to analyze the DIA data. The relative quantitative values of the altered peptides were determined by centralizing the signal intensity levels across samples.

Statistical analysis

The significant difference analysis between statistics in the figures was performed using unpaired Student's *t* test, one-way analysis of variance (ANOVA) test, or Kruskal-Wallis test. Statistical analysis was performed using SPSS software (version 20.0). Normality of the data was evaluated using the Shapiro-Wilk test. Data are presented as means ± SEM in bar graphs. Statistical significance was determined using the Bonferroni post hoc test or Dunnett's test, as indicated in the figure legends. A *P* value of less than 0.05 was considered statistically significant.

Supplementary Materials

This PDF file includes:

Figs. S1 to S4

REFERENCES

1. B. M. Burkholder, D. A. Jabs, Uveitis for the non-ophthalmologist. *BMJ* **372**, m4979 (2021).
2. S. E. Choon, A. A. Navarini, A. Pinter, Clinical course and characteristics of generalized pustular psoriasis. *Am. J. Clin. Dermatol.* **23**, 21–29 (2022).
3. M. Brüner, A. Dige, A. G. Loft, T. B. Laurberg, J. S. Agnholt, K. Clemmensen, I. McInnes, R. Lories, L. Iversen, K. F. Hjuler, T. W. Kragstrup, Spondylitis-psoriasis-enthesitis-enterocolitis-dactylitis-uveitis-peripheral synovitis (SPEED-UP) treatment. *Autoimmun. Rev.* **20**, 102731 (2021).
4. J. Chen, X. Yao, A contemporary review of Behcet's syndrome. *Clin. Rev. Allergy Immunol.* **61**, 363–376 (2021).
5. S. Teabagy, E. Wood, E. Bilsbury, S. Doherty, P. Janardhana, D. J. Lee, Ocular immunosuppressive microenvironment and novel drug delivery for control of uveitis. *Adv. Drug Deliv. Rev.* **198**, 114869 (2023).
6. H. Xu, J. V. Forrester, J. Liversidge, I. J. Crane, Leukocyte trafficking in experimental autoimmune uveitis: Breakdown of blood–retinal barrier and upregulation of cellular adhesion molecules. *Invest. Opthalmol. Vis. Sci.* **44**, 226–234 (2003).
7. W. P. Chong, M. J. Mattapallil, K. Raychaudhuri, S. J. Bing, S. Wu, Y. Zhong, W. Wang, Z. Chen, P. B. Silver, Y. Jittayasothorn, C.-C. Chan, J. Chen, R. Horai, R. R. Caspi, The cytokine IL-17A limits Th17 pathogenicity via a negative feedback loop driven by autocrine induction of IL-24. *Immunity* **53**, 384–97.e5 (2020).
8. W. Fan, X. Wang, S. Zeng, N. Li, G. Wang, R. Li, S. He, W. Li, J. Huang, X. Li, J. Liu, S. Hou, Global lactylome reveals lactylation-dependent mechanisms underlying Th17 differentiation in experimental autoimmune uveitis. *Sci. Adv.* **9**, eadh4655 (2023).
9. S. K. Wang, C. L. Cepko, Targeting microglia to treat degenerative eye diseases. *Front. Immunol.* **13**, 843558 (2022).

10. J. Huang, X. Wang, N. Li, W. Fan, X. Li, Q. Zhou, J. Liu, W. Li, Z. Zhang, X. Liu, S. Zeng, H. Yang, M. Tian, P. Yang, S. Hou, YY1 lactylation aggravates autoimmune uveitis by enhancing microglial functions via inflammatory genes. *Adv. Sci.* **11**, e2308031 (2024).
11. H. Li, B. Li, Y. Zheng, Role of microglia/macrophage polarisation in intraocular diseases (Review). *Int. J. Mol. Med.* **53**, 45 (2024).
12. Y. Okunuki, R. Mukai, T. Nakao, S. J. Tabor, O. Butovsky, R. Dana, B. R. Ksander, K. M. Connor, Retinal microglia initiate neuroinflammation in ocular autoimmunity. *Proc. Natl. Acad. Sci. U.S.A.* **116**, 9989–9998 (2019).
13. M. Prinz, T. L. Tay, Y. Wolf, S. Jung, Microglia: Unique and common features with other tissue macrophages. *Acta Neuropathol.* **128**, 319–331 (2014).
14. S. M. Silverman, W. T. Wong, Microglia in the retina: Roles in development, maturity, and disease. *Annu. Rev. Vis. Sci.* **4**, 45–77 (2018).
15. A. Hu, M. H. H. Schmidt, N. Heinig, Microglia in retinal angiogenesis and diabetic retinopathy. *Angiogenesis* **27**, 311–331 (2024).
16. E. I. Paschalis, F. Lei, C. Zhou, V. Kapoulea, A. Thanos, R. Dana, D. G. Vavvas, J. Chodosh, C. H. Dohlman, The role of microglia and peripheral monocytes in retinal damage after corneal chemical injury. *Am. J. Pathol.* **188**, 1580–1596 (2018).
17. P. Huebbe, G. Rimbach, Evolution of human apolipoprotein E (APOE) isoforms: Gene structure, protein function and interaction with dietary factors. *Ageing Res. Rev.* **37**, 146–161 (2017).
18. S. W. Barger, A. D. Harmon, Microglial activation by Alzheimer amyloid precursor protein and modulation by apolipoprotein E. *Nature* **388**, 878–881 (1997).
19. L. Qiao, J. Ma, Z. Zhang, W. Sui, C. Zhai, D. Xu, Z. Wang, H. Lu, M. Zhang, C. Zhang, W. Chen, Y. Zhang, Deficient chaperone-mediated autophagy promotes inflammation and atherosclerosis. *Circ. Res.* **129**, 1141–1157 (2021).
20. M. A. Margeta, Z. Yin, C. Madore, K. M. Pitts, S. M. Letcher, J. Tang, S. Jiang, C. D. Gauthier, S. R. Silveira, C. M. Schroeder, E. M. Lad, A. D. Proia, R. E. Tanzi, D. M. Holtzman, S. Krasemann, D. F. Chen, O. Butovsky, Apolipoprotein E4 impairs the response of neurodegenerative retinal microglia and prevents neuronal loss in glaucoma. *Immunity* **55**, 1627–44.e7 (2022).
21. J. Yin, M. Nielsen, T. Carcione, S. Li, J. Shi, Apolipoprotein E regulates mitochondrial function through the PGC-1α-sirtuin 3 pathway. *Aging* **11**, 11148–11156 (2019).
22. R. González-Domínguez, P. Castellano-Escuder, S. Lefèvre-Arbogast, D. Y. Low, A. Du Preez, S. R. Ruigrok, H. Lee, C. Helmer, M. Pallàs, M. Urpi-Sarda, A. Sánchez-Pla, A. Korosi, P. J. Lucassen, L. Aigner, C. Manach, S. Thuret, C. Samieri, C. Andres-Lacueva, Apolipoprotein E and sex modulate fatty acid metabolism in a prospective observational study of cognitive decline. *Alzheimer's Res. Ther.* **14**, 1 (2022).
23. Y. W. Kim, I. Al-Ramahi, A. Koire, S. J. Wilson, D. M. Konecki, S. Mota, S. Soleimani, J. Botas, O. Lichtarge, Harnessing the paradoxical phenotypes of APOE ε2 and APOE ε4 to identify genetic modifiers in Alzheimer's disease. *Alzheimers Dement.* **17**, 831–846 (2021).
24. H. Sies, V. V. Belousov, N. S. Chandel, M. J. Davies, D. P. Jones, G. E. Mann, M. P. Murphy, M. Yamamoto, C. Winterbourn, Defining roles of specific reactive oxygen species (ROS) in cell biology and physiology. *Nat. Rev. Mol. Cell Biol.* **23**, 499–515 (2022).
25. H. Sies, D. P. Jones, Reactive oxygen species (ROS) as pleiotropic physiological signalling agents. *Nat. Rev. Mol. Cell Biol.* **21**, 363–383 (2020).
26. D. Averill-Bates, Reactive oxygen species and cell signaling. Review. *Biochim. Biophys. Acta Mol. Cell Res.* **1871**, 119573 (2024).
27. M. Mittal, M. R. Siddiqui, K. Tran, S. P. Reddy, A. B. Malik, Reactive oxygen species in inflammation and tissue injury. *Antioxid. Redox Signal.* **20**, 1126–1167 (2014).
28. M. Scherlinger, G. C. Tsokos, Reactive oxygen species: The Yin and Yang in (auto-) immunity. *Autoimmun. Rev.* **20**, 102869 (2021).
29. Y. Ying, B. J. Padanilam, Regulation of necrotic cell death: p53, PARP1 and cyclophilin D-overlapping pathways of regulated necrosis? *Cell. Mol. Life Sci.* **73**, 2309–2324 (2016).
30. C. R. Mantel, H. A. O'Leary, B. R. Chitteti, X. X. Huang, S. Cooper, G. Hangoc, N. Brustovetsky, E. F. Srour, M. R. Lee, S. Messina-Graham, D. M. Haas, N. Falah, R. Kapur, L. M. Pelus, N. Bardeesy, J. Fitamant, M. Ivan, K.-S. Kim, H. E. Broxmeyer, Enhancing hematopoietic stem cell transplantation efficacy by mitigating oxygen shock. *Cell* **161**, 1553–1565 (2015).
31. A. Dikalova, D. Fehrenbach, V. Mayorov, A. Panov, M. Ao, L. Lantier, V. Amarnath, M. G. Lopez, F. T. Billings IV, M. N. Sack, S. Dikalov, Mitochondrial CypD acetylation promotes endothelial dysfunction and hypertension. *Circ. Res.* **134**, 1451–1464 (2024).
32. C. Zhou, M. Kuang, Y. Tao, J. Wang, Y. Luo, Y. Fu, Z. Chen, Y. Liu, Z. Li, W. Wu, L. Wang, Y. Dou, J. Wang, Y. Hou, Nynrin preserves hematopoietic stem cell function by inhibiting the mitochondrial permeability transition pore opening. *Cell Stem Cell* **31**, 1359–75.e8 (2024).
33. D. Feng, Y. Tang, H. Kwon, H. Zong, M. Hawkins, R. N. Kitsis, J. E. Pessin, High-fat diet–induced adipocyte cell death occurs through a cyclophilin D intrinsic signaling pathway independent of adipose tissue inflammation. *Diabetes* **60**, 2134–2143 (2011).
34. H. A. Itani, A. E. Dikalova, W. G. McMaster, R. R. Nazarewicz, A. T. Bikineyeva, D. G. Harrison, S. I. Dikalov, Mitochondrial cyclophilin D in vascular oxidative stress and hypertension. *Hypertension* **67**, 1218–1227 (2016).
35. J. Liu, X. Liao, N. Li, Z. Xu, W. Yang, H. Zhou, Y. Liu, Z. Zhang, G. Wang, S. Hou, Single-cell RNA sequencing reveals inflammatory retinal microglia in experimental autoimmune uveitis. *MedComm (2020)* **5**, e534 (2024).
36. N.-W. Fan, J. Li, S. K. Mittal, W. Foulsham, E. Elbasiony, R. M. Huckfeldt, S. K. Chauhan, Y. Chen, Characterization of clinical and immune responses in an experimental chronic autoimmune uveitis model. *Am. J. Pathol.* **191**, 425–437 (2021).
37. C. Dello Russo, N. Cappoli, I. Coletta, D. Mezzogori, F. Paciello, G. Pozzoli, P. Navarra, A. Battaglia, The human microglial HMC3 cell line: Where do we stand? A systematic literature review. *J. Neuroinflammation* **15**, 259 (2018).
38. O. Kann, F. Almouhanna, B. Chausse, Interferon γ: A master cytokine in microglia-mediated neural network dysfunction and neurodegeneration. *Trends Neurosci.* **45**, 913–927 (2022).
39. Y. Iitani, R. Miki, K. Imai, K. Fuma, T. Ushida, S. Tano, K. Yoshida, A. Yokoi, H. Kajiyama, T. Kotani, Interleukin-17A stimulation induces alterations in microglial microRNA expression profiles. *Pediatr. Res.* **95**, 167–173 (2024).
40. A. C. Murphy, S. J. Lalor, M. A. Lynch, K. H. G. Mills, Infiltration of Th1 and Th17 cells and activation of microglia in the CNS during the course of experimental autoimmune encephalomyelitis. *Brain Behav. Immun.* **24**, 641–651 (2010).
41. G. K. Nanayakkara, H. Wang, X. Yang, Proton leak regulates mitochondrial reactive oxygen species generation in endothelial cell activation and inflammation—A novel concept. *Arch. Biochem. Biophys.* **662**, 68–74 (2019).
42. H. Xian, K. Watari, E. Sanchez-Lopez, J. Offenberger, J. Onyuru, H. Sampath, W. Ying, H. M. Hoffman, G. S. Shadel, M. Karin, Oxidized DNA fragments exit mitochondria via mPTP- and VDAC-dependent channels to activate NLRP3 inflammasome and interferon signaling. *Immunity* **55**, 1370–85.e8 (2022).
43. A. Mary, R. Mancuso, M. T. Heneka, Immune activation in Alzheimer disease. *Annu. Rev. Immunol.* **42**, 585–613 (2024).
44. N. Hagemeyer, K.-M. Hanft, M.-A. Akriditou, N. Unger, E. S. Park, E. R. Stanley, O. Staszewski, L. Dimou, M. Prinz, Microglia contribute to normal myelinogenesis and to oligodendrocyte progenitor maintenance during adulthood. *Acta Neuropathol.* **134**, 441–458 (2017).
45. A. Borrajo, C. Spuch, M. A. Penedo, J. M. Olivares, R. C. Agís-Balboa, Important role of microglia in HIV-1 associated neurocognitive disorders and the molecular pathways implicated in its pathogenesis. *Ann. Med.* **53**, 43–69 (2021).
46. M. Schwabenland, W. Brück, J. Priller, C. Stadelmann, H. Lassmann, M. Prinz, Analyzing microglial phenotypes across neuropathologies: A practical guide. *Acta Neuropathol.* **142**, 923–936 (2021).
47. M. Sharma, P. Pal, S. K. Gupta, Microglial mediators in autoimmune uveitis: Bridging neuroprotection and neurotoxicity. *Int. Immunopharmacol.* **136**, 112309 (2024).
48. F. Lei, N. Cui, C. Zhou, J. Chodosh, D. G. Vavvas, E. I. Paschalis, CSF1R inhibition by a small-molecule inhibitor is not microglia specific; affecting hematopoiesis and the function of macrophages. *Proc. Natl. Acad. Sci. U.S.A.* **117**, 23336–23338 (2020).
49. O. Butovsky, H. L. Weiner, Microglial signatures and their role in health and disease. *Nat. Rev. Neurosci.* **19**, 622–635 (2018).
50. R. W. Mahley, Central nervous system lipoproteins. *Arterioscler. Thromb. Vasc. Biol.* **36**, 1305–1315 (2016).
51. T. Vogels, A.-N. Murgoci, T. Hromádka, Intersection of pathological tau and microglia at the synapse. *Acta Neuropathol. Commun.* **7**, 109 (2019).
52. C. M. Kloske, C. J. Barnum, A. F. Batista, E. M. Bradshaw, A. M. Brickman, G. Bu, J. Dennison, M. D. Gearon, A. M. Goate, C. Haass, M. T. Heneka, W. T. Hu, L. K. L. Huggins, N. S. Jones, R. Koldamova, C. A. Lemere, S. A. Liddelow, E. Marcora, S. E. Marsh, H. M. Nielsen, K. K. Petersen, M. Petersen, S. D. Piña-Escudero, W. Q. Qiu, Y. T. Quiroz, E. Reiman, C. Sexton, M. G. Tansey, J. Tcw, C. E. Teunissen, B. M. Tijms, R. van der Kant, R. Wallings, S. C. Weninger, W. Wharton, D. M. Wilcock, T. J. Wishard, S. L. Worley, H. Zetterberg, M. C. Carrillo, APOE and immunity: Research highlights. *Alzheimers Dement.* **19**, 2677–2696 (2023).
53. A. A. Johnson, A. Stolzing, The role of lipid metabolism in aging, lifespan regulation, and age-related disease. *Aging Cell* **18**, e13048 (2019).
54. L. C. Lee, M. Q. L. Goh, E. H. Koo, Transcriptional regulation of APP by apoE: To boldly go where no isoform has gone before. *Bioessays* **39**, 10.1002/bies.201700062 (2017).
55. Y. Taguchi, E.-G. Lee, J. Tulloch, S. Chen, L. Leong, A. D. Saxton, B. Kraemer, M. Darvas, C. D. Keene, A. Shutes-David, K. Todd, S. Millard, C.-E. Yu, Redefining transcriptional regulation of the APOE gene and its association with Alzheimer's disease. *PLOS ONE* **15**, e0227667 (2020).
56. M. S. Haney, R. Pálovics, C. N. Munson, C. Long, P. K. Johansson, O. Yip, W. Dong, E. Rawat, E. West, J. C. M. Schlachetzki, A. Tsai, I. H. Guldner, B. S. Lamichhane, A. Smith, N. Schaum, K. Calcuttawala, A. Shin, Y.-H. Wang, C. Wang, N. Koutsodendris, G. E. Serrano, T. G. Beach, E. M. Reiman, C. K. Glass, M. Abu-Remaileh, A. Enejder, Y. Huang, T. Wyss-Coray, APOE4/4 is linked to damaging lipid droplets in Alzheimer's disease microglia. *Nature* **628**, 154–161 (2024).
57. M. Cui, C. Cheng, L. Zhang, High-throughput proteomics: A methodological mini-review. *Lab. Invest.* **102**, 1170–1181 (2022).
58. L. Zheng, X. Chen, X. He, H. Wei, X. Li, Y. Tan, J. Min, M. Chen, Y. Zhang, M. Dong, Q. Yin, M. Xue, L. Zhang, D. Huo, H. Jiang, T. Li, F. Li, X. Wang, X. Li, H. Chen, METTL4-mediated mitochondrial DNA N6-methyldeoxyadenosine promoting macrophage inflammation and atherosclerosis. *Circulation* **151**, 946–965 (2025).

59. Y. Tsujimoto, S. Shimizu, Role of the mitochondrial membrane permeability transition in cell death. *Apoptosis* **12**, 835–840 (2007).
60. H. Fan, H. Tian, F. Jin, X. Zhang, S. Su, Y. Liu, Z. Wen, X. He, X. Li, C. Duan, CypD induced ROS output promotes intracranial aneurysm formation and rupture by 8-OHdG/NLRP3/MMP9 pathway. *Redox Biol.* **67**, 102887 (2023).
61. A. Mendoza, P. Patel, D. Robichaux, D. Ramirez, J. Karch, Inhibition of the mPTP and lipid peroxidation is additively protective against I/R injury. *Circ. Res.* **134**, 1292–1305 (2024).
62. S.-I. Bibli, A. Papapetropoulos, E. K. Iliodromitis, A. Daiber, V. Randriamboavonjy, S. Steven, P. Brouckaert, A. Chatzianastasiou, K. E. Kypreos, D. J. Hausenloy, I. Fleming, I. Andreadou, Nitroglycerine limits infarct size through S-nitrosation of cyclophilin D: A novel mechanism for an old drug. *Cardiovasc. Res.* **115**, 625–636 (2019).
63. J.-i. Koga, R. Umezu, Y. Kondo, T. Shirouzu, N. Orkhonselenge, H. Ueno, S. Katsuki, T. Matoba, Y. Nishimura, M. Kataoka, Cyclophilin D induces necrotic core formation by mediating mitochondria-associated macrophage death in advanced atherosclerotic lesions. *Atherosclerosis* **396**, 118524 (2024).
64. G. Paulsson, X. Zhou, E. Törnquist, G. K. Hansson, Oligoclonal T cell expansions in atherosclerotic lesions of apolipoprotein E-deficient mice. *Arterioscler. Thromb. Vasc. Biol.* **20**, 10–17 (2000).
65. F. Bonacina, D. Coe, G. Wang, M. P. Longhi, A. Baragetti, A. Moregola, K. Garlaschelli, P. Uboldi, F. Pellegatta, L. Grigore, L. Da Dalt, A. Annoni, S. Gregori, Q. Xiao, D. Caruso, N. Mitro, A. L. Catapano, F. M. Marelli-Berg, G. D. Norata, Myeloid apolipoprotein E controls dendritic cell antigen presentation and T cell activation. *Nat. Commun.* **9**, 3083 (2018).
66. J. Zhao, T. C. Ikezu, W. Lu, J. R. Macyczko, Y. Li, L. J. Lewis-Tuffin, Y. A. Martens, Y. Ren, Y. Zhu, Y. W. Asmann, N. Ertekin-Taner, T. Kanekiyo, G. Bu, APOE deficiency impacts neural differentiation and cholesterol biosynthesis in human iPSC-derived cerebral organoids. *Stem Cell Res. Ther.* **14**, 214 (2023).
67. J. E. Pankiewicz, A. M. Lizińczyk, L. A. Franco, J. R. Diaz, M. Martá-Ariza, M. J. Sadowski, Absence of apolipoprotein E is associated with exacerbation of prion pathology and promotes microglial neurodegenerative phenotype. *Acta Neuropathol. Commun.* **9**, 157 (2021).
68. M. Rudolf, G. Malek, J. D. Messinger, M. E. Clark, L. Wang, C. A. Curcio, Sub-retinal drusenoid deposits in human retina: Organization and composition. *Exp. Eye Res.* **87**, 402–408 (2008).
69. Y. Huang, R. W. Mahley, Apolipoprotein E: Structure and function in lipid metabolism, neurobiology, and Alzheimer's diseases. *Neurobiol. Dis.* **72**, 3–12 (2014).
70. R. W. Read, G. N. Holland, N. A. Rao, K. F. Tabbara, S. Ohno, L. Arellanes-Garcia, P. Pivetti-Pezzi, H. H. Tessler, M. Usui, Revised diagnostic criteria for Vogt-Koyanagi-Harada disease: Report of an international committee on nomenclature. *Am. J. Ophthalmol.* **131**, 647–652 (2001).
71. A. Lewin, L. Tian, P. Yang, B. Lei, J. Shao, C. Wang, Q. Xiang, L. Wei, Z. Peng, A. Kijlstra, AAV2-mediated subretinal gene transfer of hIFN-α attenuates experimental autoimmune uveoretinitis in mice. *PLOS ONE* **6**, e19542 (2011).
72. X. Liu, J. Meng, X. Liao, Y. Liu, Q. Zhou, Z. Xu, S. Yin, Q. Cao, G. Su, S. He, W. Li, X. Wang, G. Wang, D. Li, P. Yang, S. Hou, A de novo missense mutation in MPP2 confers an increased risk of Vogt-Koyanagi-Harada disease as shown by trio-based whole-exome sequencing. *Cell. Mol. Immunol.* **20**, 1379–1392 (2023).
73. H. J. Lin, C. C. Wei, C. Y. Chang, T. H. Chen, Y. A. Hsu, Y. C. Hsieh, H. J. Chen, L. Wan, Role of chronic inflammation in myopia progression: Clinical evidence and experimental validation. *EBioMedicine* **10**, 269–281 (2016).

Acknowledgments

Funding: This work was supported by the National Natural Science Foundation Project of China (82271078 and 82530033 to S.H. and 82271061 to F.L.), the Beijing Municipal Public Welfare Development and Reform Pilot Project for Medical Research Institutes (PWD&RPP-MRI, JYY2023-6), and the Beijing Young Scholar Program (no. 076). **Author contributions:** Writing—original draft: S.Z., S.H., and F.L. Conceptualization: S.Z., S.H., and F.L. Investigation: S.Z., Y.W., X.L., W.F., S.H., and F.L. Writing—review and editing: S.H. and F.L. Methodology: S.Z., Y.W., X.L., F.C., B.C., C.W., S.H., and F.L. Resources: S.H., F.L., K.H., and H.F. Funding acquisition: S.H. and F.L. Data curation: S.Z., Y.W., S.H., and F.L. Validation: S.Z., H.F., F.C., B.C., C.W., K.H., S.H., and F.L. Supervision: S.H., F.L., and K.H. Formal analysis: S.Z., Y.W., S.H., and F.L. Software: S.H. and F.L. Project administration: S.H. and F.L. Visualization: S.Z., Y.W., W.F., X.L., S.H., and F.L. **Competing interests:** The authors declare that they have no competing interests. **Data and materials availability:** The scRNA-seq data are openly available in the Gene Expression Omnibus (GSE191260). The RNA sequencing and proteomics data are openly available in the Dryad repository (dataset doi: 10.5061/dryad.37pvmcvzx). All other data and code needed to evaluate and reproduce the results in the paper are present in the paper and/or the Supplementary Materials. No other scripts and software were used other than those mentioned in Materials and Methods.

Submitted 12 August 2025
Accepted 25 November 2025
Published 1 January 2026
10.1126/sciadv.aeb3991